Evaluating the potential to monitor aboveground biomass in forest and oil palm in Sabah, Malaysia, for 2000–2008 with Landsat ETM+ and ALOS-PALSAR

Alexandra C. Morel [a] , Joshua B. Fisher [b] & Yadvinder Malhi [a]

[a] Oxford University Centre for the Environment (OUCE), Environmental Change Institute, University of Oxford, Oxford, UK

[b] NASA Jet Propulsion Laboratory, California Institute of Technology, Pasadena, CA, USA

Available online: 31 Jan 2012

PLEASE SCROLL DOWN FOR ARTICLE

Taylor & Francis
Taylor & Francis Group

Evaluating the potential to monitor aboveground biomass in forest and oil palm in Sabah, Malaysia, for 2000–2008 with Landsat ETM+ and ALOS-PALSAR

ALEXANDRA C. MOREL*†, JOSHUA B. FISHER‡
and YADVINDER MALHI†

†Oxford University Centre for the Environment (OUCE), Environmental Change Institute, University of Oxford, Oxford, UK
‡NASA Jet Propulsion Laboratory, California Institute of Technology, Pasadena, CA, USA

We explored the potential of Landsat Enhanced Thematic Mapper (ETM+) imagery to quantify the expansion of planted oil palm area and changes in aboveground biomass (AGB) in plantation and forest in Sabah, Malaysian Borneo, from 2000 to 2008. For comparison, a classification layer derived from an Advanced Land-Observing Satellite Phased Array type L-band Synthetic Aperture Radar (ALOS-PALSAR) Fine Beam Dual (FBD)-polarized mosaic from 2008 was used for change detection analysis. Field-measured AGB values from 85 ha of forest and oil palm plantation plots were compared with 12 vegetation indices (VIs) and four spectral mixture analysis (SMA) derivatives. Correlations against indices using optical data were higher for oil palm biomass than for forest biomass. Change detection analysis of forest conversion to oil palm plantation was performed for areas designated as protected areas, commercial forest reserve and areas with no forest-use designation. This analysis found an increase in oil palm area of 38% (1450 km^2) and a total decrease in forest area of 13.1% (1900 km^2) for the whole study area from 2000 to 2008. The greatest area of forest loss was in areas not designated as forest reserve by the Sabah Forestry Department, although some oil palm expansion was detected in both commercial and protected areas. Using derived equations for biomass, we estimated that 46.6 Tg of carbon dioxide equivalents (CO$_2$e) were released in these three forest designations or 53.4 Tg CO$_2$e for the entire study area due to forest conversion to oil palm. These results are presented as relevant for on-going efforts to remotely monitor the carbon emission implications of forest loss as part of the United Nations Framework Convention on Climate Change's (UNFCCC's) proposed mechanism, Reduced Emissions from Deforestation and Degradation (REDD).

1. Introduction

Southeast Asia is home to 20% of the world's remaining tropical rainforest, but is among the regions with the highest rates of deforestation (Geist and Lambin 2002). Tropical deforestation degrades air quality, reduces biodiversity (Myers *et al.* 2000), causes long-term socioeconomic losses and impacts the global carbon cycle (Defries *et al.* 2002). Over the last 145 years, it has been estimated that 33.5 Pg carbon (C)

*Corresponding author. Email: alexandra.morel@gmail.com

(122.8 Pg CO_2e) has been emitted from forest conversion to permanent agriculture, and 11.5 Pg C (42.2 Pg CO_2e) from forest degradation; carbon accumulation in plantation areas was 1.5 Pg C (5.5 Pg CO_2e), primarily since 1980 (Houghton and Hackler 1999). In Asia, 30% of land-cover change was due to direct conversion of intact forest to large-scale permanent agriculture, primarily for timber extraction (Chomitz *et al*. 2006). Fifty-five studies addressing the drivers of deforestation in Asia were reviewed by Geist and Lambin (2002), revealing that there was 100% incidence of agriculture following deforestation in Asian forests. Rates of deforestation are following the trends in urban population growth and agricultural commodity exports (Defries *et al*. 2010).

Planted hectares of oil palm have been expanding rapidly across Southeast Asia, especially in Malaysia and Indonesia. Sabah, a state in Malaysian Borneo, has had a rapid increase in oil palm plantation area over the past 30 years (figure 1) and is currently the state with the most planted hectares in Malaysia (Malaysian Palm Oil Board (MPOB) 2008). This large-scale conversion has led to the loss of lowland Dipterocarp forest (McMorrow *et al*. 1996) and was a major contributor in conjunction with El-Niño Southern Oscillation (ENSO) to the rampant forest fires in 1997–1998 (McMorrow and Talip 2001). Although oil palm plantations are perennial crops, they store significantly less aboveground biomass (AGB) than intact and logged forest, averaging ~75 Mg C ha^{-1} (275 Mg CO_2e ha^{-1}) over their 25-year lifetime (Murdiyarso *et al*. 2002, Henson and Chang 2003, Danielsen *et al*. 2008). Intact forest and logged forest can have AGB values greater than 250 Mg C ha^{-1} (917 Mg CO_2e ha^{-1}) or 150 Mg C ha^{-1} (550 CO_2e ha^{-1}), respectively, resulting in a significant carbon loss due to forest conversion to oil palm plantation. As a result, the 'carbon debt' or the time necessary to compensate (by biofuel substitution of fossil fuel combustion) for the initial carbon loss may be more than 85 years (Danielsen *et al*. 2008, Fargione *et al*. 2008a). Most studies that have estimated this change are assuming an AGB typical of primary forests prior to conversion; however, the carbon
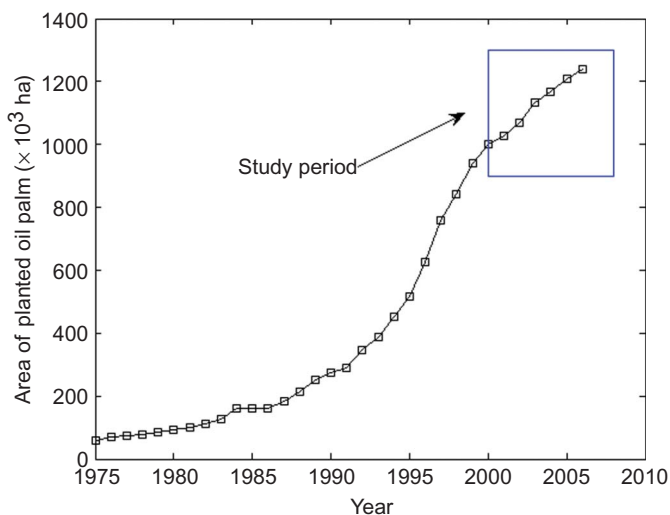

Figure 1. Expansion of the planted area of oil palm in Sabah, Malaysia, between 1975 and 2007 (MPOB 2008). The time period of the current study is highlighted.

balance from conversion of severely degraded forest to oil palm plantation can be much lower. Hence, there is a need to improve the monitoring capability of AGB in this region to provide better estimates of carbon storage in vegetation. Improving these estimates will aid in the implementation of the United Nations Framework Convention on Climate Change's (UNFCCC's) proposed Reduced Emissions from Deforestation and Degradation (REDD) mechanism, which is explored further in §4.

Oil palms (*Elaeis guineensis*), as perennial trees, have a canopy structure more similar to a forest than other agricultural crops; therefore, the remote sensing of oil palms can be based on methods for forest monitoring (McMorrow 2001). For oil palm, researchers have used high-resolution (4 m), hyper-spectral (Jusoff and Pathan 2009) and Landsat Thematic Mapper (TM) imagery to map plantation distributions and/or ages. Thenkabail *et al*. (2004) mapped AGB of oil palm plantations and groves using high-resolution IKONOS imagery in West Africa with reasonable success (coefficient of determination, R^2, values of 0.62–0.72). Relating the reflectance to AGB in tropical regions has been a challenge to researchers since Sader *et al*. (1989) attempted to correlate the normalized difference vegetation index (NDVI) derived from Landsat TM to tropical AGB in Puerto Rico. Since then, monitoring AGB studies have been undertaken in both temperate (Muukkonen and Heiskanen 2005, Balzter *et al*. 2007, Zheng *et al*. 2007) and tropical (Foody *et al*. 2003, Lu 2005, Lu *et al*. 2005) regions using a variety of sensors. Mapping AGB in tropical regions is challenging due to the complex canopy structure, predominant cloud cover and dense biomass. Optical data can capture the canopy in only two dimensions, missing the important sub-canopy structure (Anaya *et al*. 2009); therefore, optical approaches have been considered limited for estimating AGB relative to the Synthetic Aperture Radar (SAR) and light detection and ranging (LiDAR) (Foody *et al*. 2001, Patenaude *et al*. 2005, Gibbs *et al*. 2007). These limitations can be ameliorated by using multiple bands, by modelling canopy 'greenness' using either vegetation indices (VIs) (Sader *et al*. 1989, Foody *et al*. 2001, Phua and Saito 2003, Zheng *et al*. 2004, Lu 2005) or spectral mixture analysis (SMA) (Lu *et al*. 2004a, Souza *et al*. 2005). SMA and VIs are preferable for AGB mapping as they can minimize the influence of topography, soil reflectance and atmospheric attenuation (Lu 2006). SMA, in particular, utilizes the benefits of multi-spectral, reflectance data, providing a spectral signature for different land-cover categories (GOFC-GOLD 2009). To date, SMA has been used mainly for monitoring the occurrence of forest degradation in real time but has not been related to AGB. This technique may be particularly useful for estimating AGB of oil palm due to the sub-pixel occurrence of soil and shade as the canopy closes with age.

This article has three main aims, which are to evaluate the potential of using Landsat Enhanced Thematic Mapper (ETM+) imagery to (1) differentiate between oil palm and forest areas using land-cover classification, (2) estimate and map AGB in oil palm and forest areas using satellite-derived indices and (3) to estimate gross changes in forest area and/or AGB values due to the expansion of oil palm areas for 2000–2008 inside and outside forest reserves. Advanced Land-Observing Satellite Phased Array type L-band Synthetic Aperture Radar (ALOS-PALSAR) images are used for classification comparison. This study will contribute to the literature by applying SMA analysis for AGB estimation, estimating oil palm biomass from medium (30 m) resolution imagery and attempting to estimate the carbon footprint of oil palm expansion at the landscape scale using remote sensing.

2. Materials and methods

2.1 *Study site*

The study area covered much of eastern, lowland Sabah, where annual precipitation ranges from 2000 to 3000 mm. The climate of the region is influenced by two monsoons acting in November–March and June–July, with a relative dry season in April–September, although monthly precipitation levels rarely drop below 100 mm (Marsh and Greer 1992). Temperatures are typical for a moist, tropical climate, rarely going below 20°C or above 30°C in the lowlands, with an annual mean of 26.7–27.7°C. The lowland forest is moist tropical and dominated by the *Dipterocarpaceae* family, with over 180 species of this family in Sabah alone (Whitmore 1984). The sampled forest area ranged from mixed Dipterocarp forest, both protected and logged, heath forest (a.k.a. *kerangas*) and some areas of peat swamp forest (see figure 2). Two species, *Acacia mangium* and *Albizia ferrucania*, cultivated in timber plantations were sampled from the Sabah Softwoods Sendirian Berhad (SSSB) site, 70 km north of Tawau. Plantations of oil palm, *E. guineensis*, were sampled from Wilmar International Limited's (formerly PPB Plantations') plantations located near Sandakan. Figure 2 shows the sampled forest reserves and the locations of specific plots; however, land-cover change analysis and biomass estimates were made over a larger area of Sabah depending on the coverage of Landsat imagery.

2.2 *Field data*

Over 100 ha of ground data were analysed for this study collected during 2007 and 2008 across lowland Sabah. Stratified sampling was performed by disturbance level
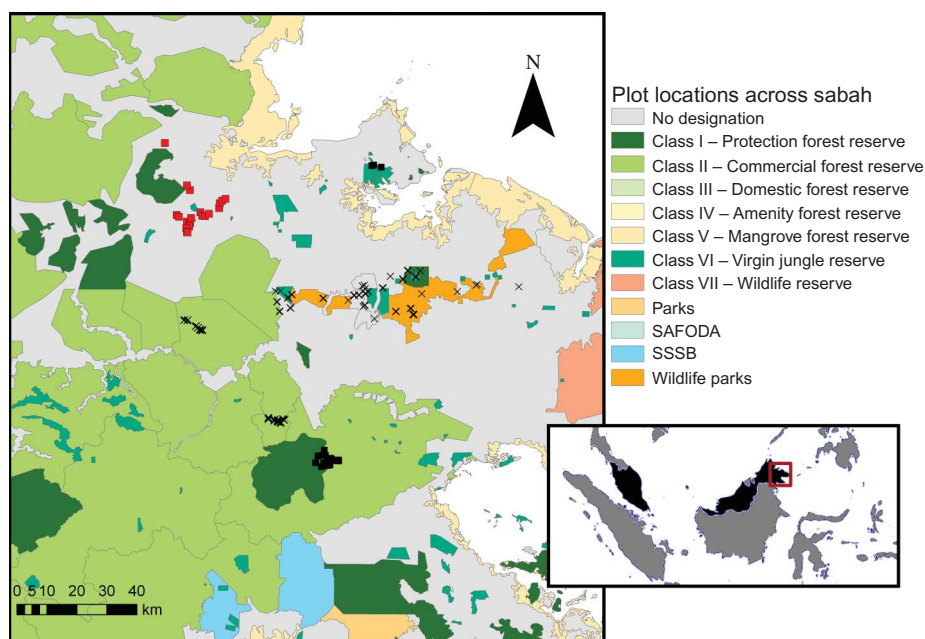

Figure 2. Forest reserve types for Sabah, Malaysian Borneo, and location of sampled forest and plantations. Black crosses indicate transects, black squares refer to square plot sites and red squares designate oil palm plots sampled for this study.

(high, medium and low) across forest types (listed above) and year of logging activity in lowland Dipterocarp forest (e.g. 1970, 1988–1989, 1995–1996, 2000–2002, 2003–2006, 2007) in order to sample a suitable range of AGB estimates, although it was not possible to take into account the intensity of logging as these data were not available. Sampling of oil palm plantation was stratified by age, across four age classes; however, all plots were located in a region of similar management, limiting their applicability for representing non-industrial oil palm areas. These data were collected as line transects (20 m × 250–1200 m), 0.25 ha (50 m × 50 m) square plots and 1 ha square plots (100 × 100 m). While line transects were not directly comparable to a pixel as a primary sampling unit, they did provide a measure of forest heterogeneity in a site. For line transects, tree measurements were made for all trees that met the minimum size requirements within 10 m of either side of a straight line following a cardinal direction. These measurements were grouped into sub-plots every 10 m along the line for per-hectare biomass estimates to be calculated at a number of different scales (see figure 3). For all measurements, trees were identified to species or genus, in order to estimate wood density. Height measurements were taken for a subset of trees in a plot or transect and then estimated for all trees using a plot-specific generated, allometric equation related to diameter at breast height (DBH). Due to cloud cover and gaps in post-2003 Landsat ETM+ scan-line corrector (SLC)-off data, not all ground plots were usable. Therefore, only 85 ha of field data were used for analysis, listed in table 1 by land-cover classification and per-hectare biomass estimates.

Per-hectare AGB estimates were derived for trees with ≥10 cm DBH using the allometric equation for moist, tropical forest from Chave *et al*. (2005):

Continue for 250 m,
500 m or 750 m

10 m

10 m

10 m
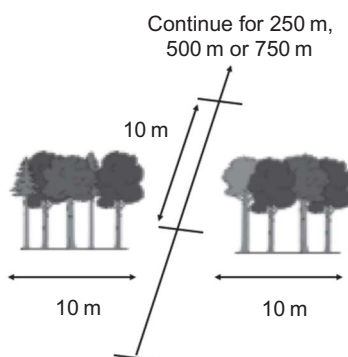
Figure 3. Schematic for line transect sampling. Measurements were made 10 m either side of a 250–750 m long line transect. Markers were placed every 10 m along the line and all tree measurements were grouped by marker (tree images from Börner *et al*. (2010)).

Table 1. Analysed field data plot areas classified by biomass value.

Land-cover class	Biomass (Mg C ha^{-1}) [CO$_2$e]	Area (ha)
Intact forest	>250 [> 917]	21.6
Logged forest	150–250 [550–917]	29.4
Degraded forest/mature plantation	10–150 [37–550]	29.4
Immature oil palm plantation	< 10 [< 37]	5
Total		85.3

$$AGB = \rho e^{(-1.499+2.148InD+0.207InD^2-0.02081InD^3)}, \tag{1}$$

where ρ is the species-specific (e.g. *Shorea hypoleuca*) wood density taken from the literature (Brown 1997, ICRAF 2008) and D is the measured DBH. AGB estimates for oil palm plantations were derived from field measurements and equations developed by Corley and Tinker (2003), which involved the combining of trunk and frond AGB estimates per palm and summing them for a hectare estimate. The following three equations were used for these estimates:

$$AGB_{trunk} = 100\pi(rz)^2 h\rho, \tag{2}$$

where r is the radius of the trunk (in cm) without frond bases, z is the ratio of the trunk diameter below frond bases to the measured diameter above frond bases (estimated to be 0.777 from sampled trunks), h is the height of the trunk (in m) to the base of the fronds, ρ is the trunk density (in kg m^{-3}) dependent on the age, x, in years of the palm:

$$\rho = \frac{(0.0076x + 0.083)}{100}, \tag{3}$$

$$AGB_{frond} = 0.102Id + 0.21, \tag{4}$$

where l is the length of the petiole (in cm) and d is the depth of petiole (in cm). The petiole of the most recently cut frond was measured for each palm to generate this estimate.

2.3 *Imagery*

There are several optical and radar sensors that have been assessed for monitoring AGB. The Landsat series of sensors provide the longest continuous data set of surface reflectance of any sensor and, therefore, are useful for land-cover change analysis. Landsat imagery has a resolution of 30 m, which is a reasonable grain size for estimating the forest cover (Hansen *et al*. 2008, Zheng *et al*. 2008). The key challenges to using Landsat imagery are atmospheric correction, cloud frequency, intervals between sampling and image gaps due to sensor malfunction. These challenges are specifically addressed in this article. We were unable to locate Landsat TM images, which did not have the added problem of gaps, for the same time period due to limited archiving of this data set (USGS 2003).

Four Landsat ETM+ scenes were required to include all field plots, comprising paths 116 and 117 and rows 56 and 57. Due to the largely aseasonal climate, 'cloud-free' images were collected across an entire year to generate one annual composite. Annual composites were created for 2000 and 2008 from 3 to 4 images per scene depending on availability. Gap-filling of the 2008 mosaic with 2003 data was considered but not performed due to the time difference and the speed of land-cover change in this region. Ninety-metre digital elevation data were taken from the Shuttle Radar Topographic Mission (SRTM) (USGS 2006), registered to each Landsat scene and resampled to 30 m resolution.

Finally, a two-class classification image for 2008 derived from ALOS-PALSAR Fine Beam Dual (FBD) imagery was used for comparison with Landsat ETM+ classification and for subsequent change analysis.

2.3.1 Image preprocessing. Landsat digital numbers (DNs) were corrected to ground reflectance using the LandCor atmospheric correction framework developed by Zelazowski *et al*. (2011). The method performs pixel-by-pixel corrections using the 6S radiative transfer code (Vermote *et al*. 1997), which generates specific look-up tables for relevant aerosol, water vapour and altitude conditions. For diurnal aerosol and water vapour estimates, images of the Moderate Resolution Imaging Spectroradiometer (MODIS) joint Atmosphere Product Level 2 (MODATML2) were acquired for each date of a collected Landsat scene. Date-specific relationships between atmospheric pressure (modelled from the SRTM digital elevation data) and the atmospheric aerosol or water vapour content were generated. The MODATML2 is a product from the Terra platform and, therefore, has a data set running from 13 October 2000.

Unfortunately, in 2003, the Landsat ETM+ SLC malfunctioned and subsequently all captured images have lost 22% of their land-cover data due to widening horizontal gaps ranging from 2 to 14 pixels (Zhang *et al*. 2007). There are methods to infill the missing data; however, regardless of the correction method used, the applicability of Landsat ETM+ for spatially explicit monitoring of forest change has been severely compromised (Trigg *et al*. 2006). We attempted to gap-fill using several images from the same year; however, gap-filling was less effective from the centre to the edge of the scene due to the widening gaps in each image. We considered gap-filling using data from an historical SLC-on image (before May 2003) and either a segment-based or a histogram-based correction (Wulder *et al*. 2008). However, due to the significant time period between 2003 and 2008, attempts at filling in the 2008 data proved unsuccessful and were deemed unnecessary for initial evaluation of this monitoring method. Instead, cloud-free pixels were combined from all images of the same year to provide a reasonable, in-filled composite for each scene. The best pixels were selected using Band 1 and NDVI, to remove cloud pixels and choose higher vegetation values across images.

To improve classification accuracy, eight scenes of ALOS-PALSAR FBD imagery were acquired, processed to σ^0 (power) values and 30 m resolution as well as terrain corrected using the Alaska Satellite Facility's (ASF's) Mapready software and a 90 m SRTM digital elevation model (Jarvis *et al*. 2006). The images were then orthorectified to Universal Transverse Mercator (UTM) projection using Landsat ETM+ imagery, with a root mean square error (RMSE) of < 0.65 Landsat pixels. Finally, a three-pixel, enhanced Lee filter was applied to reduce speckle in the images (Lee 1980). For maximum likelihood classification (MLC), a three-band image consisting of the bands HH, HV and a ratio of HV/HH (to reduce topographic effects) was analysed. Half of the oil palm and forest points were used as training data and the other half for evaluating the accuracy of the MLC method.

2.3.2 Vegetation indices. An extensive literature review was performed to identify existing VIs and select a subset, based on their characteristics (e.g. dominance in the literature, number of bands used, sensitivity to atmospheric attenuation), for this study. Table 2 lists the indices chosen, their equations and reference. NDVI is

Table 2. Vegetation indices with equation and literature source.

Vegetation index (VI)	Equation	Source	Benefits
Simple ratio (SR)	$SR = \dfrac{[NIR]}{[R]}$	Birth and McVey (1968)	Commonly used VI
Normalized difference vegetation index (NDVI)	$NDVI = \dfrac{([NIR] - R)}{([NIR] + R)}$	Rouse *et al.* (1973)	Most commonly used VI in the literature
Soil-adjusted vegetation index (SAVI)	$SAVI = \dfrac{(1 + L)\,([NIR] - R)}{[NIR] + R + L}$ where L is set to 1.0 for very low vegetation, 0.5 for intermediate and 0.25 for dense vegetation	Huete (1988)	Corrects for background reflectance of soil
Perpendicular vegetation index (PVI)	$PVI = \dfrac{([NIR] - aR - b)}{\sqrt{(1 + a^2)}}$ where the 'soil line' is represented as $NIR = aR + b$	Richardson and Everitt (1992)	Corrects for background reflectance of soil, using a scene-derived 'soil line'
Corrected normalized difference vegetation index (CNDVI)	$CNDVI = \dfrac{[NIR] - R}{[NIR] + R}\left[1 - \dfrac{([SWIR] - [SWIR_{min}])}{([SWIR_{max}] - [SWIR_{min}])}\right]$	Nemani *et al.* (1993)	Improves saturation threshold of NDVI with dense vegetation
Soil and atmospherically resistant vegetation index (SARVI)	$SARVI = \dfrac{(1 + L)\,([NIR] - R_B)}{([NIR] + R_B + L)}$ where $R_B = R - \gamma\,(B - R)$, γ = function to correct the red channel radiance, L as described above	Huete *et al.* (1997)	Corrects for background reflectance of soil and atmospheric attenuation

(*Continued*)

Table 2. (*Continued.*)

Vegetation index (VI)	Equation	Source	Benefits
Aerosol-free vegetation index (AFRI)	$\text{AFRI7} = \dfrac{([\text{NIR}] - \frac{1}{2}[\text{SWIR}_{2.1}])}{([\text{NIR}] + \frac{1}{2}[\text{SWIR}_{2.1}])}$ $\text{AFRI5} = \dfrac{([\text{NIR}] - \frac{1}{3}[\text{SWIR}_{1.6}])}{([\text{NIR}] + \frac{1}{3}[\text{SWIR}_{1.6}])}$	Karnieli *et al.* (2001)	VI that corrects for atmospheric attenuation due to aerosols
Infrared index (IRI)	$\text{IRI} = \dfrac{([\text{NIR}] - [\text{SWIR}_{1.6}])}{([\text{NIR}] + [\text{SWIR}_{1.6}])}$	McMorrow (2001)	Found to have the highest relation to oil palm age
Enhanced vegetation index (EVI)	$\text{EVI} = \dfrac{([\text{NIR}] - R)}{([\text{NIR}] + R + B)}$	Huete *et al.* (2002)	Exhibits increased sensitivity to canopy variations
Linearized NDVI (LNDVI)	$\text{LNDVI} = \dfrac{4}{\pi}\arctan(\text{NDVI})$	Ünsalan and Boyer (2004)	Improves saturation threshold of NDVI with dense vegetation
Atmospherically resistant vegetation index (ARVI)	$\text{ARVI} = \dfrac{([\text{NIR}] - 2R + B)}{([\text{NIR}] + 2R - B)}$	Lu *et al.* (2004)	VI that takes account of atmospheric attenuation

Notes: *B* is the reflectance of the 'blue' band (0.45–0.52 μm); *R* is the reflectance of the 'red' band (0.63–0.69 μm); NIR is the reflectance in the near-infrared (0.77–0.90 μm); SWIR (1.55–1.75 and 2.08–2.35 μm) is the reflectance in the short-wave infrared; SWIR_{min} and SWIR_{max} refer to the minimum and maximum reflectances observed in field plots; $\text{SWIR}_{2.1}$ and $\text{SWIR}_{1.6}$ are bands 7 and 5 with wavelengths 2.1 and 1.6 μm, respectively.

among the most widely used VI in the remote-sensing literature due to its reduction of topographic effects and its normalized linear relationship between the red (R) and near-infrared (NIR) reflectance bands (Silleos *et al*. 2006). Although it has not been found to be a reliable VI for mapping areas of dense biomass (e.g. tropical forest) (Sader *et al*. 1989, Huete *et al*. 1997, Foody *et al*. 2001, Lu *et al*. 2004b), it has been included for comparison.

The two NDVI variants in table 2 are intended to improve the problem with saturation of the VI in the case of dense vegetation (Ünsalan and Boyer 2004) and reduce the issue of background effects, such as soil, by using the short-wave infrared (SWIR) bands (Heiskanen 2006). The corrected normalized difference vegetation index (CNDVI) is one of the best performing VIs in temperate settings (Zheng *et al*. 2004), chiefly when it is possible to separate areas by structural characteristics (e.g. hardwoods and conifers). This is not always possible in tropical areas where species composition is particularly complex, but analysis was performed separately for forest and oil palm areas. The soil-adjusted vegetation index (SAVI) and perpendicular vegetation index (PVI) are best able to reduce background effects (Lu *et al*. 2004b), with the former performing best with dense vegetation due to its wide dynamic range and lower sensitivity to atmospheric attenuation (Mcdonald *et al*. 1998). Both have been described by Jackson and Huete (1991) as *distance-based* VIs, whereby the scatter of R and NIR reflectance in a 2D space is used by the VI to include the 'distance' of the pixel reflectance from bare soil. The use of the 'soil line' is most explicitly utilized in PVI. Two soil lines were used to generate the PVI: PVI1 used the equation derived for each scene, while PVI2 used the relationship developed by Heiskanen (2006). Finally, the infrared index (IRI) was included because McMorrow (2001) found that the inclusion of the SWIR band had the strongest correlation with oil palm stand age. All VIs were generated for each scene and their values extracted for all plot sites that did not fall in a gap or a cloud pixel in order to be correlated with biomass estimates. These equations were solved for AGB resulting in the use of equation (5) for mapping biomass:

$$\text{AGB} = e^{\left(\frac{v1-b}{m}\right)}, \tag{5}$$

where VI refers to the pixel value of the index, b is the intercept and m is the slope of the derived logarithmic regression between AGB and reflectance.

2.3.3 Spectral mixture analysis. In addition to comparing biomass relationships with generated VIs, SMA was performed on each composite. The principal of SMA is that the spectral signature of each pixel within a scene is a weighted mixture, often assumed to be linear, of component endmembers or 'pure pixels' (Huete 1986). Equation (6) describes the model:

$$d_{ik} = \sum_{j=1}^{n} r_{ij}c_{jk}, \tag{6}$$

where d_{ik} is the measured spectra for spectral mixture k in waveband i, n is the number of endmembers in the mixture, j is the number of the endmember, r_{ij} is the reflectance

from endmember j in waveband i and c_{jk} is the weighted contribution from endmember j for spectral mixture k, which must sum to one. The primary endmembers used for vegetation mapping are green vegetation (GV), non-photosynthetically active vegetation (NPV), shade (S_1) and soil (S_2) (Roberts *et al*. 1993, Souza *et al*. 2005); however, SMA has been performed with fewer endmembers (Lu *et al*. 2004a). SMA has been used successfully for mapping land-cover change (Anderson *et al*. 2005, Ferreira *et al*. 2007), canopy damage due to selective logging (Asner and Heidebrecht 2002, Souza *et al*. 2005, Broadbent *et al*. 2006) and regeneration of forest due to succession (Hall *et al*. 1991) in the tropics. It has also been paired with MLC to improve land-cover classification accuracy (Lu *et al*. 2004a).

The four endmembers described above can be combined to calculate the normalized difference fraction index (NDFI), which is defined by the group GOFC-GOLD (2009) as the most reliable method for mapping areas of degraded forest and canopy damage. It has not been used previously for estimating carbon stocks. Once the spectral endmembers of a scene have been found and fraction images for each generated, the GV image is normalized to the shade image (equation (7)):

$$GV_{shade} = \frac{GV}{(1 - S_1)}. \tag{7}$$

Once a new fraction image, GV_{shade}, has been generated, the NDFI can be calculated using equation (8):

$$NDFI = \frac{GV_{shade} - (NPV + S_2)}{GV_{shade} + NPV + S_2}. \tag{8}$$

For this study, the four endmembers were extracted using the Sequential Maximum Angle Convex Cone (SMACC) algorithm available in the Environment for Visualizing Images (ENVI) 4.6 software (ENVI: Research Systems, Boulder, CO, USA), which automatically identifies a specified number of extreme pixels from the data's spectral cloud. The four endmembers representing GV, non-photosynthetic vegetation, shade and soil were chosen by their spectra and are presented in figure 4. The spectral signature of GV and non-photosynthetic vegetation can be differentiated by the disparity in reflectance 'peaks' between the red and NIR bands. The non-photosynthetic vegetation spectra exhibit higher reflectance in the red region, due to a lack of chlorophyll. The shade spectra show little reflectance in any wavelength. This automatic method did have a difficulty in sensing soil pixels, as the resulting soil spectra is not as bright in the shorter wavelengths as expected; however, it does show increasing reflectance with longer wavelengths (e.g. NIR and SWIR bands). Again, NDFI values and values for its components (GV, GV_{shade}, non-photosynthetic vegetation and shade) were extracted for each plot site. Analysis performed on both NDFI and VIs required taking the means of all pixels within a plot area in order to reduce noise from pixel heterogeneity. Correlations were performed between land-cover data and the logarithm of biomass estimates generated from 1 ha plot estimates. Finally, RMSEs were calculated for significant relationships to assess their efficacy in predicting AGB, and biomass maps were attempted from the most significant relationships with oil palm and forest AGB.
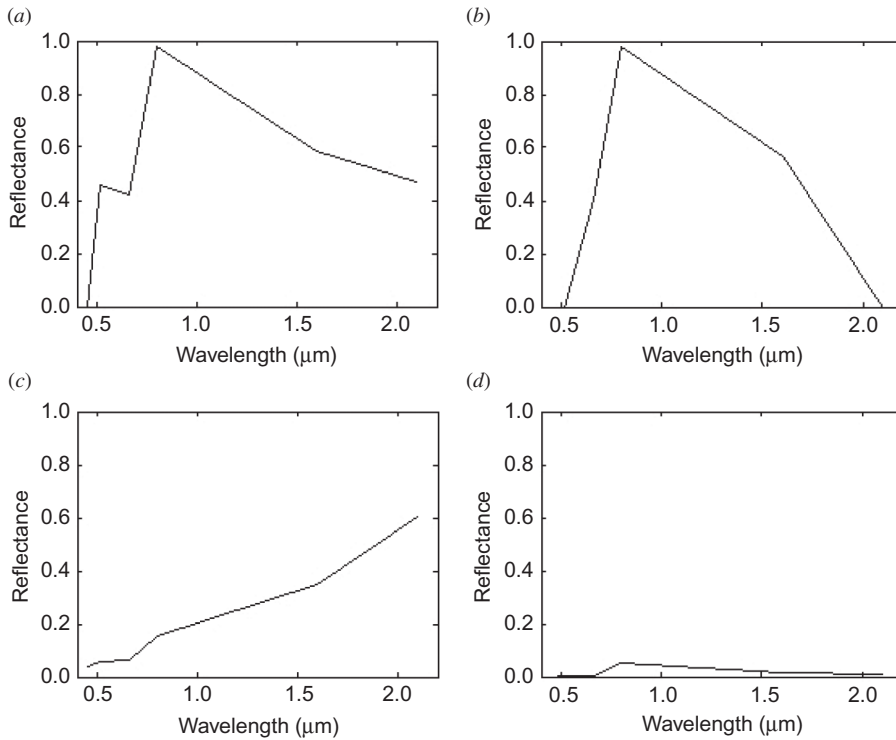
Figure 4. Spectral signatures for the four endmembers of vegetation, generated by ENVI's SMACC algorithm. (*a*) The typical spectral signature for non-photosynthetic vegetation (e.g. reflection in the red band), (*b*) the typical spectral signature for green vegetation, (*c*) the spectral signature for soil, though with lower than expected reflectance in the visible spectrum, and (*d*) the spectral signature for shade.

2.3.4 Land-cover classification. Classification of vegetation into structural types before estimating AGB is often necessary, due to the different behaviour of these surfaces with optical reflectance data and their ability to store biomass (Anaya *et al.* 2009). We applied both unsupervised (*k*-means) and supervised (maximum likelihood) classification techniques followed by a decision-tree classifier to improve final classification layers in mountainous regions. The *k*-means unsupervised technique is based on the establishment of an initial set of land-cover classes with pixels classed iteratively, keeping class means within a set standard deviation (Tou and Gonzalez 1974). The MLC algorithm is a parametric, supervised classification technique that assumes equal probability of a pixel's class, unless separate class weightings are assigned (Hagner and Reese 2007). When analysing noisy, SLC-off Landsat data, MLC can be the better technique, as well as reducing the number of land-cover classes to improve overall accuracy (Bédard *et al.* 2008).

Unsupervised (*k*-means) and supervised (MLC) classifications were performed using all six bands of the 2000 and 2008 composites. Both classifications used three land-cover classes, with intact and logged forest combined from table 1, and two classes, only oil palm and forest. For unsupervised classification, ten classes were identified before being combined into either three or two classes. Because the majority of

field plots were within two scenes ((1) path 17, row 56 and (2) path 117, row 57), only classifications of these images are presented. The ground points were initially split evenly between training and testing of the MLC algorithm; however, due to the range of reflectance values for each land-cover type and the reduced number of usable ground points, only using half of the available points resulted in an overestimate of forest areas. Therefore, all points were needed for training and testing, thereby reducing the reliability of this sensor for land-cover classification. For comparison, an MLC classification of oil palm and forest pixels was performed on a 2008 mosaic of SAR data from the ALOS-PALSAR sensor over the same region. This layer produced a more reliable classification of mountainous areas (due to using a ratio of the two polarized bands HH/HV to reduce topographic effects). Due to poor classification accuracy in mountainous areas in Landsat scenes, a decision-tree classifier was used to change areas likely misclassified as oil palm to forest where the slope was greater than $25°$ and altitude was greater than 500 m and where areas in forest reserves had been classified as forest in the 2008 ALOS-PALSAR layer. Finally, all classifications were automatically segmented with ENVI to remove erroneously classified pixels within large areas of forest or oil palm. Confusion matrices were derived for each layer using a pixel-to-pixel sampling protocol.

   The more accurate of the two 2008 classification layers was used to select pixels from the 2000 composite that had changed from forest to oil palm plantation and to estimate the AGB of that pixel in 2000 and 2008. Images were resampled to 100 m resolution using ENVI's orthorectification module before AGB estimates were calculated, to more closely approximate 1 ha AGB calculations. Gross changes in AGB were estimated by subtracting per pixel AGB estimates in 2000 and 2008; however, to calculate differences in oil palm and forest AGB, values were converted to CO_2 equivalents (CO_2e) due to their different carbon content values. Oil palm has a carbon content of 45% of dry biomass and forest wood is often approximated as 50%. The conversion of carbon to CO_2e is accomplished by multiplying by the molar ratio of 44/12.

3.   Results

Forest plots and oil palm plantation plots (collected at 0.25 ha) were analysed separately, with significant linear regression results for all VIs (table 3). The best performing VIs were CNDVI, which had the widest dynamic range, while PVI1, PVI2 and the atmospherically resistant vegetation index (ARVI) exhibited slight, bimodal distributions (results not shown), indicating these indices are discerning differences in land cover. Also, PVI1 and PVI2 had identical R^2 values, showing that the slope of the soil line was not important to derive for each image; however, the inclusion of the soil line itself appears to be well suited for monitoring oil palm plantations. Surprisingly, IRI did not exhibit a significant relationship with oil palm biomass, as it had been included specifically for its inclusion of SWIR shown to have a strong relationship with oil palm age (McMorrow 2001). RMSE values reveal the poor predictive power of these VIs for AGB estimates in forest; however, RMSE values in oil palm plantations were reasonable (although 35 Mg ha^{-1} can constitute from 30% to 100% of AGB values in oil palm plantations, depending on age).

   The same analysis as above was performed for the SMA technique, NDFI and three of its components (table 4). The soil abundance image was not analysed as it had very few values in the plot areas and, as discussed above, had analytical limitations. In forest plots, the NPV component exhibits the strongest relationship with biomass,

Table 3. R^2 and RMSE values for linear regression analysis of each VI to the logarithm of biomass for all oil palm plots and 1 ha forest plots.

Vegetation index	Oil palm plots		Forest plots	
	R^2	RMSE	R^2	RMSE
AFVI5	–	–	–	–
AFVI7	–	–	–	–
ARVI	0.69**	34.8	–	–
CNDVI	0.61**	35.6	0.15**	1777.4
EVI	–	–	–	–
LNDVI	–	–	–	–
NDVI	–	–	0.06	1778.7
PVI1	0.76*	35.9	0.08*	1778.1
PVI2	0.76*	36.0	0.08*	1778.3
SAVI	–	–	–	–
SR	–	–	0.12**	1779.8
IRI	–	–	–	–

Note: All reported numbers are significant with * and ** indicating *p*-values of 0.01 and 0.001, respectively.

Table 4. R^2 and RMSE values for linear regression analysis of NDFI and each NDFI component to the logarithm of biomass for all oil palm plots and 1 ha forest plots.

NDFI and components	Oil palm		Forest	
	R^2	RMSE	R^2	RMSE
NDFI	0.58**	32.4	0.16**	1763.1
GV	0.41*	34.7	0.09*	1769.7
NPV	0.78**	35.3	**0.22****	1771.2
Shade	**0.80****	35.5	0.17**	1771.6

Note: All reported numbers are significant with * and ** indicating *p*-values of 0.01 and 0.001, respectively. Bold numbers indicate strongest relationships used for AGB estimates.

and NDFI and the shade component exhibit similar significance. NDFI endmembers perform much better in the oil palm plots, though GV was the poorest performing endmember, in forest and oil palm plots. These RMSE values were similar to VI results for oil palm plantations and forest plots, respectively, with NDFI producing the lowest errors of all SMA derivatives. NPV and shade were the best endmembers to describe biomass in forest and oil palm plantations, respectively (figure 5). The relationships were perhaps due to the simple canopy structure of an oil palm monoculture exhibiting increasing shade fractions with greater canopy closure and, for forest, visible non-photosynthetic vegetation decreasing with increasingly dense forest. The equations used for subsequent AGB calculations in units of $CO_2e\ ha^{-1}$ were (the subscripts are self-explanatory)

$$\text{AGB}_{\text{forest}} = 0.5 \left(\frac{44}{12} \right) e^{\left(\frac{\text{NPV} - 0.13297}{-0.0086681} \right)}. \tag{9}$$
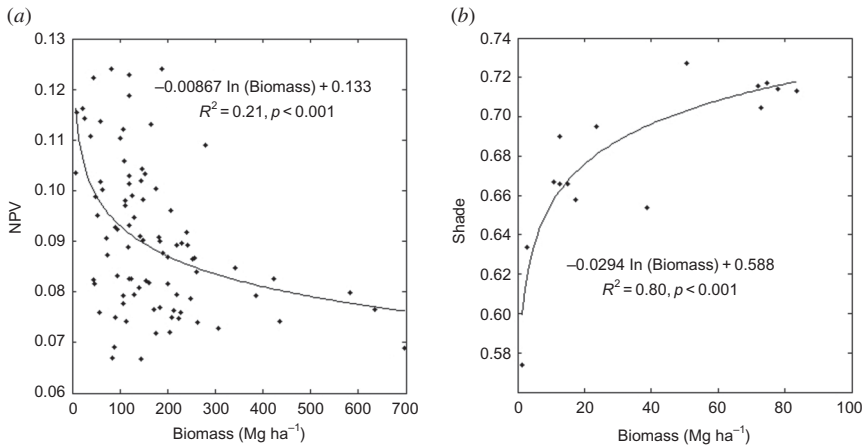
Figure 5. Linear regressions for NDFI components and the logarithm of AGB. (*a*) The relationship between forest AGB and non-photosynthetic vegetation and (*b*) the relationship between oil palm AGB and shade.

$$\text{AGB}_{\text{oil\_palm}} = 0.45 \left(\frac{44}{12}\right) e^{\left(\frac{S_1 - 0.5877}{0.029436}\right)}. \tag{10}$$

As mentioned above, two classification techniques were used on the 2008 composite, though only the two-class MLC results for the Landsat ETM+ and ALOS-PALSAR mosaics are presented (figure 6). The 2008 Landsat image had a classification accuracy of 69.7% and κ (kappa coefficient) of 0.21, after segmentation, compared to an accuracy of 97.0% and $\kappa = 0.64$ in the SAR image (see table 5). For both layers, the user's accuracy for oil palm classification was significantly lower than for forest, 54.5% and 54.0%, respectively for the Landsat and ALOS scene. This is due to the high commission rates, or false positives, of areas classified as oil palm in both layers. Classification using three classes had significantly lower accuracies and, therefore, are not presented or used. Supervised and unsupervised classification of the 2000 imagery were performed using 2008 field plots; therefore, it was not possible to differentiate forest plots by AGB values, but instead classification using only two classes was accomplished. After segmentation and the decision-tree classifier, the classification accuracy was 74.1% and $\kappa = 0.24$. However, this classification seemed to misclassify many forest areas (particularly mountainous ones) as oil palm; by assuming that areas classified as forest in the 2008 SAR within areas designated as forest were also forest in 2000, classification accuracy was improved to 97.8% and $\kappa = 0.87$ (figure 7). For this layer, the classification of oil palm had a high producer's and user's accuracy, compared to the 2008 classification layers presented above.

Change detection was performed between the two MLC classification layers, in areas designated as commercial or protected forest reserve and land areas with no formal designation. The areas without a formal forest designation by the state may be zoned for agriculture or urban development, and therefore, highly likely to be planted with oil palm. The results of these two analyses are presented in table 6, which show an overall decrease in the forest area of 13.1% (1935 km^2) and an increase in oil palm area of 38% (1450 km^2). However, the errors in these estimates are revealed through
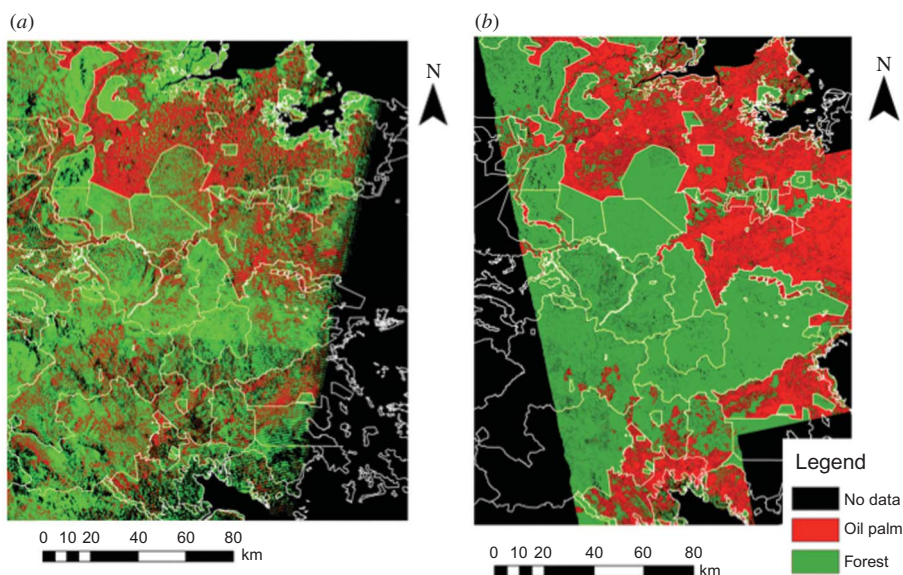
Figure 6. Map of vegetation cover in 2008 for the study area derived from supervised maximum likelihood classification with two land-cover classes for Landsat imagery (overall accuracy 69.7% and $\kappa = 0.21$) (*a*) and for ALOS-PALSAR FBD imagery (overall accuracy 97.2% and $\kappa = 0.65$) (*b*).

Table 5. Assessment of classification accuracy for each classification layer.

Confusion matrices results	Landsat (2008)		ALOS (2008)		Landsat (2000)	
	Oil palm	Forest	Oil palm	Forest	Oil palm	Forest
Producer's accuracy (%)	89.1	68.5	100.0	97.0	97.8	97.8
User's accuracy (%)	54.4	99.9	54.0	100.0	81.5	99.8
Overall accuracy (%)	69.7		97.0		97.8	
Kappa coefficient	0.21		0.64		0.87	

the producer's and user's accuracies discussed above. Analysis of the classification layers' confusion matrices indicates that some areas of oil palm have been misclassified in both layers and, therefore, overestimated for the year 2008.

Areas without a formal designation exhibited a 55.2% (1780 km^2) decrease in forest and a 40% increase in oil palm (1290 km^2). Forest losses in both protected and commercial forest reserves were significantly lower, 3.7% and 8.6%, respectively, with increases in oil palm area of 79 and 80 km^2, respectively. While noteworthy, most of this conversion is focused in one or two reserves, or else is the result of some oil palm cultivation along the edges of designated forest reserves (especially if forest reserve borders were not 100% accurate). The areas of change are presented in figure 7. While the area analysed is a subset of Sabah's total area, this estimated increase in oil palm area is similar to the MPOB's statistics (see figure 1), which report an increase in oil palm area of 33% over the same time period for all of Sabah (compared to the 38% increase reported here for a subset of the state of Sabah).
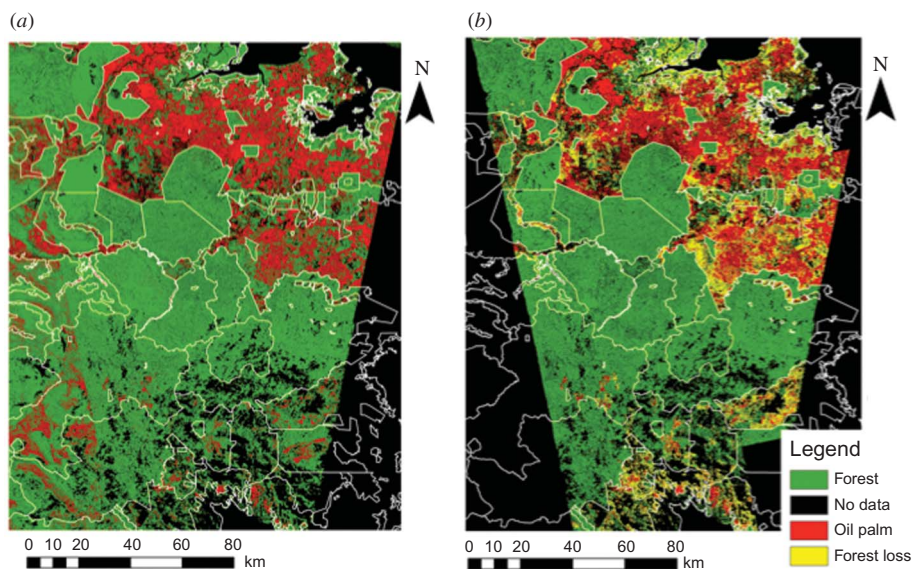
Figure 7. (*a*) Supervised maximum likelihood classification for 2000 Landsat mosaic, hilly areas corrected to ALOS-FBD SAR forest area, for two classes (overall accuracy 97.8% and $\kappa = 0.87$) and (*b*) change in forest and oil palm area between 2000 Landsat and 2008 ALOS-FBD SAR classifications. The areas indicated as forest and oil palm in the change image did not change from 2000 to 2008, whereas yellow indicates areas of forest converted to oil palm. See figure 2 for protection or management status of each forest area.

Using equations (9) and (10) and resampled 100 m resolution imagery, AGB values were calculated for change pixels (e.g. pixels classified as forest in 2000 and oil palm in 2008) using shade and NPV fraction images derived from Landsat ETM+. As RMSE values were very high for forest AGB, the values presented in table 7 are only rough estimates, with considerable errors reported. The total change in AGB, which includes carbon sequestration by oil palms, was estimated to be 53.4 Tg CO_2e for the entire study area or 46.6 Tg CO_2e within the three areas of forest designations analysed separately. Calculations were also performed of solely forest carbon 'lost' since 2000 as policy proposals regarding biofuels do not intend to include carbon sequestration from palm plantations in land-use change estimates, in which case a total of 68.4 Tg CO_2e were released. Finally, for comparison with previous carbon debt analyses, average hectare values were calculated for changes in AGB values, forest and oil palm AGB estimates for the three different forest designations. Again, the range of estimates was too large to make any reliable conclusions; however, their implications are discussed.

4. Discussion

This study presented analysis of 12 VIs and the first use of the GOFC-GOLD-endorsed NDFI for estimating AGB in tropical forests. Most VIs poorly described forest AGB; however, background effects, such as soil reflectance and atmospheric attenuation, by using the blue or SWIR bands, were important factors to include. The most consistent VI was CNDVI, which has been successfully used for mapping temperate AGB, especially after vegetation was separated by structure (Zheng *et al*. 2004). NDFI and its components provided a stronger relationship in forests than other VIs,

Table 6. Percentage change and area change statistics for oil palm and forest areas between 2000 and 2008 for areas without a forest reserve classification ('no designation') and for areas classified as commercial forest reserve and protected.

Final stage ALOS (2008)	Initial stage Landsat (2000)					
	Forest			Oil palm		
	Change (%)					
Classes	No designation	Commercial reserves	Protected areas	No designation	Commercial reserves	Protected areas
Unclassified	17.7	25.4	27.7	14.1	91.1	64.2
Oil palm	55.2	0.9	3.7	70.7	8.9	35.8
Forest	27.1	73.7	68.6	15.3	0.0	0.0
Class difference	−55.2	−8.6	−3.7	40.0	16.4	76.0
	Area change (km²)					
Unclassified	570.7	2385.4	595.1	452.2	445.7	66.9
Oil palm	1775.6	80.3	79.1	2269.4	43.5	37.3
Forest	871.8	6919.4	1475.8	490.4	0.0	0.0
Class difference	−1775.6	−80.3	−79.1	1285.2	80.3	79.1
Total change (%)		−13.1			38.0	
Total area change (km²)		−1935.1			1444.7	

Notes: All change statistics are calculated from the 2000 classification. All pixels classified as forest or oil palm in 2000 are broken down into 2008 classes. Class differences for oil palm and forest are calculated after removing unclassified pixels, in order to only estimate verifiable changes. The lower rows present the percentage change and area change across all forest designations for forest and oil palm.

Table 7. Estimates of aboveground carbon changes from shade and NPV biomass equations for oil palm and forest pixels, with very high standard deviation values.

Factor	Total (incl. other designations)	No designation	Commercial reserve	Protected area
Change in aboveground carbon 2000–2008 (Tg CO_2e)	−53.4	−46.2	−0.3	−0.1
Forest carbon loss from 2000 (Tg CO_2e)	−68.4	−59.5	−3.2	−0.2
Mean hectare forest carbon 2000 (Mg CO_2e ha^{-1})	394.2 ± 334.4	394.5 ± 334.3	452.1 ± 326.7	497.2 ± 318.6
Mean hectare oil palm carbon 2008 (Mg CO_2e ha^{-1})	86.2 ± 114.0	87.6 ± 112.6	407.0 ± 294.1	268.8 ± 288.2
Mean hectare change in carbon 2000–2008 (Mg CO_2e ha^{-1})	−308.0 ± 346.1	−306.5 ± 345.4	−45.1 ± 32.6	−228.1 ± 359.7

although it appeared to be limited by high saturation in the GV fraction image; this measure should be explored further in other AGB monitoring studies (Souza *et al*. 2005, GOFC-GOLD 2009).

Better correlations for mapping AGB in this region have been found using an artificial neural network (ANN) using all Landsat TM bands (Foody *et al*. 2001); however, this method of analysis relies on extensive training data and the results for one image may not be applicable for images from previous years. Therefore, as this study was focused on estimating the change in AGB, an ANN approach was not pursued. The RMSE values for both VIs and NDFI components were similar and unreasonably large for modelling forest AGB. Therefore, efforts to quantify the changes in AGB are meant to be illustrative rather than definitive.

Nevertheless, two of this article's three aims have been accomplished. While not as effective without SAR data, Landsat ETM+ is able to differentiate between oil palm areas and forested areas. Without using the SAR classification layer as an additional information input, areas with significant topography as well as areas of mature oil palm plantations and degraded forest were misclassified. The latter finding is consistent with McMorrow's (2001) study where she found estimating stand age of oil palm the most difficult for mature plantations. However, high commission rates indicate that the differentiation between forest and oil palm can be further improved. This is likely to be due to the SAR layer exhibiting similar backscatter for swamp forest and oil palm plantation. Therefore, future studies in this region will need adequate ground points of both land covers. While AGB values in forest are poorly modelled, AGB values in oil palm plantation exhibited high levels of correlation to several VIs and SMA derivatives. The shade fraction provided the most significant relationship, making it the strongest candidate for modelling oil palm AGB. Therefore, this study does show that Landsat ETM+-derived indices are able to produce similar, if not more significant, correlations with oil palm AGB than high-resolution (e.g. 4 m) imagery, such as IKONOS analysed by Thenkabail *et al*. (2004).

To select the forest and oil palm pixels to be analysed, change detection analysis was used to estimate forest loss. Compared to state-wide MPOB (2008) statistics (see figure 1), the combined SAR and Landsat analysis appeared to provide a reasonable estimate of oil palm expansion. Due to the significant increase in classification accuracy after correcting misclassified oil palm pixels with SAR data, it appears necessary to combine these data sets for reliable change detection. On the other hand, as SAR data are unable to discern AGB in oil palm plantations (Morel *et al.* 2011), SMA of Landsat ETM+ provides a useful means of estimating this parameter. This data set could be combined with SAR-based forest AGB estimates for a complete AGB map of this study area; however, as the ALOS-PALSAR sensor has only been in orbit since 2006, it provides little opportunity for meaningful historical estimation of AGB changes at present. As a result, this analysis was attempted with Landsat ETM+ data; however, in future, this analysis would be improved as a hybrid approach.

The NPV fraction saturates in areas of high biomass; therefore, it is unlikely that it will ever be able to reliably estimate AGB values in dense forest. Undisturbed forests in this region can reach AGB values of 400–500 Mg dry biomass ha^{-1} (730–900 Mg CO_2e ha^{-1}) (Yamakura *et al*. 1986, Murdiyarso *et al*. 2002, Paoli *et al*. 2008, Slik *et al*. 2010), with even logged areas maintaining AGB values greater than 200 Mg ha^{-1} (or 360 Mg CO_2e ha^{-1}) (Morel *et al.* 2011), although Foody *et al*. (2001) measured logged forest AGB values as low as 64 Mg ha^{-1} (or 118 Mg CO_2e ha^{-1}). This analysis indicates that forest areas replaced by oil palm have similar AGB values to logged forest, far below the intact forest AGB values. This is not surprising, as these planted areas generally follow timber extraction and/or forest degradation due to other causes (Chomitz *et al*. 2006); therefore, studies that have assumed AGB values for relatively undisturbed forest (Danielsen *et al*. 2008, Fargione *et al*. 2008b) may be overestimating the emissions that can be attributed directly to oil palm expansion.

This study is directly relevant to the on-going development of the UNFCCC's REDD mechanism, designed to harness carbon payments for forest conservation. Uncertainty in forest degradation monitoring is particularly problematic for the implementation of REDD. Hence, there remain several challenges for reliable monitoring of this mechanism, in terms of both technical (Patenaude *et al*. 2005, Gibbs *et al*. 2007, Olander *et al*. 2008) and political barriers (Venning 2010). However, this study contributes to the remote-sensing field by exploring the application of the SMA-derived index, NDFI, for estimating changes in forest AGB, which has been advocated by the GOFC-GOLD. While measured forest plots in this study may have saturated the signal with high AGB values, change estimates suggest much of the forests in this region are degraded and further estimates to monitor this phenomenon would be valuable. Finally, reporting requirements for the sustainability rules of the European Union's Renewable Energy Directive (EU 2009) do not allow the inclusion of carbon sequestration by biofuel feedstock crops, such as oil palm. However, the calculations presented in table 7 reveal there is a significant discrepancy if oil palm carbon is not included. Whether or not this indicates an overestimation of carbon emissions appears to be primarily a political decision.

From this analysis, it is clear that the majority of emissions from forest conversion to oil palm plantation in Sabah occurred in areas not designated to remain forest by the state. This would indicate that governance of these forest reserves has been relatively robust. While the detection of some oil palm in commercial forest reserves and protected areas is somewhat alarming, their respective contributions to emissions from land-use change in the region are very small. Also, as vectors of forest reserve

boundaries may not be precise, it would be necessary to verify on the ground whether areas converted to oil palm were planted illegally before too many conclusions can be drawn.

5. Conclusions

The results of this study suggest Landsat ETM+, on its own, is not an ideal sensor for monitoring changes in AGB, particularly in the dense, tropical forests of Borneo. One of the major limitations is due to the gaps resulting from the SLC failure as well as the inherent limited ability of an optical sensor to perceive sub-canopy structure, such as biomass. Monitoring of biomass of oil palm areas, on the other hand, was significantly better, with NDFI and its components providing slightly better models for AGB. For forest, VIs and SMA techniques offered little analytical value for this study. The combination of optical data and SAR data produced the most robust estimate of land-cover change for years before the launch of ALOS-PALSAR (pre-2007), indicating that monitoring of total land-cover change can be attempted, although future studies in this region would benefit from initial state forest AGB estimates from SAR data instead of Landsat NDFI components.

This study has produced estimates of emissions from forest conversion to oil palm plantation; however, these are only meant to illustrate both the range of AGB values captured across land-cover types and the relatively low AGB values in forest being converted to oil palm plantations. Belowground biomass has not been quantified, nor have areas of peatland, which are uncommon in Sabah. However, as estimates of emissions from land-use change need to be improved, particularly for this region, methods that account for changes in soil carbon and land-cover monitoring that differentiates forest on mineral and organic soils will be needed.

References

ANAYA, J.A., CHUVIECO, E. and PALACIOS-ORUETA, A., 2009, Aboveground biomass assessment in Colombia: a remote sensing approach. *Forest Ecology and Management*, **257**, pp. 1237–1246.

ANDERSON, L.O., SHIMABUKURO, Y.E. and ARAI, E., 2005, Multitemporal fraction images derived from Terra MODIS data for analysing land cover change over the Amazon region. *International Journal of Remote Sensing*, **26**, pp. 2251–2257.

ASNER, G.P. and HEIDEBRECHT, K.B., 2002, Spectral unmixing of vegetation, soil and dry carbon cover in arid regions: comparing multispectral and hyperspectral observations. *International Journal of Remote Sensing*, **23**, pp. 3939–3958.

BALZTER, H., ROWLAND, C.S. and SAICH, P., 2007, Forest canopy height and carbon estimation at Monks Wood National Nature Reserve, UK, using dual-wavelength SAR interferometry. *Remote Sensing of Environment*, **108**, pp. 224–239.

BÉDARD, R., REICHERT, G., DOBBINS, R. and TRÉPANIER, I., 2008, Evaluation of segment-based gap-filled Landsat ETM+ SLC-off satellite data for land cover classification in southern Saskatchewan, Canada. *International Journal of Remote Sensing*, **29**, pp. 2041–2054.

BIRTH, G.S. and McVEY, G., 1968, Measuring the color of growing turf with a reflectance spectrophotometer. *Agronomy Journal*, **60**, pp. 640–643.

BÖRNER, A., BELLASSEN, V. and LUYSSAERT, S., 2010, *Forest Management Cartoons* (Germany/France: MPI-BGC/LSCE). Available online at: http://www.lsce.ipsl.fr/Pisp/124/sebastiaan.luyssaert.html

BROADBENT, E.N., ZARIN, D.J., ASNER, G.P., PEÑA-CLAROS, M., COOPER, A. and LITTELL, R., 2006, Recovery of forest structure and spectral properties after selective logging in lowland Bolivia. *Ecological Applications*, **16**, pp. 1148–1163.

BROWN, S., 1997, Estimating biomass and biomass change of tropical forests: a primer. In *Forestry Paper 134*, F. R. A. Publication (Ed.) (Rome: FAO).

CHAVE, J., ANDALO, C., BROWN, S., CAIRNS, M.A., CHAMBERS, J.Q., EAMUS, D., FÖLSTER, H., FROMARD, F., HIGUCHI, N., KIRA, T., LESCURE, J.P., NELSON, B.W., OGAWA, H., PUIG, H., RIÉRA, B. and YAMAKURA, T., 2005, Tree allometry and improved estimation of carbon stocks and balance in tropical forests. *Oecologia*, **V145**, pp. 87–99.

CHOMITZ, K., BUYS, P., LUCA, G., THOMAS, T. and WERTZ-KANOUNNIKOFF, S., 2006, *At Loggerheads? Agricultural Expansion, Poverty Reduction and Environment* (Washington, DC: The World Bank).

CORLEY, R.H.V. and TINKER, P.B., 2003, *The Oil Palm* (Oxford: Blackwell Science Ltd.).

DANIELSEN, F., BEUKEMA, H., BURGESS, N.D., PARISH, F., BRUHL, C.A., DONALD, P.F., MURDIYARSO, D., PHALAN, B., REIJNDERS, L., STRUEBIG, M. and FITZHERBERT, E.B., 2008, Biofuel plantations on forest lands: double jeopardy for biodiversity and climate. *Conservation Biology*, **23**, pp. 348–358.

DEFRIES, R.S., HOUGHTON, R.A., HANSEN, M.C., FIELD, C.B., SKOLE, D. and TOWNSHEND, J., 2002, Carbon emissions from tropical deforestation and regrowth based on satellite observations for the 1980s and 1990s. *Proceedings of the National Academy of Sciences of the United States of America*, **99**, pp. 14256–14261.

DEFRIES, R.S., RUDEL, T., URIARTE, M. and HANSEN, M., 2010, Deforestation driven by urban population growth and agricultural trade in the twenty-first century. *Nature Geoscience*, **3**, pp. 178–181.

EU, 2009, Directive 2009/28/EC of the European Parliament and of the Council of 23 April 2009 on the promotion of the use of energy from renewable sources and amending and subsequently repealing Directives 2001/77/EC and 2003/30/EC, OJ L 140, pp. 16–62. Available online at: http://eur-lex.europa.eu/LexUriServ/LexUriServ.do?uri=CELEX:32009L0028:en:NOT

FARGIONE, J., HILL, J., TILMAN, D., POLASKY, S. and HAWTHORNE, P., 2008a, Biofuels: effects on land and fire: response. *Science*, **321**, p. 199.

FARGIONE, J., HILL, J., TILMAN, D., POLASKY, S. and HAWTHORNE, P., 2008b, Land clearing and the biofuel carbon debt. *Science*, **319**, pp. 1235–1238.

FERREIRA, M.E., FERREIRA, L.G., SANO, E.E. and SHIMABUKURO, Y.E., 2007, Spectral linear mixture modelling approaches for land cover mapping of tropical savanna areas in Brazil. *International Journal of Remote Sensing*, **28**, pp. 413–429.

FOODY, G.M., BOYD, D.S. and CUTLER, M.E.J., 2003, Predictive relations of tropical forest biomass from Landsat TM data and their transferability between regions. *Remote Sensing of Environment*, **85**, pp. 463–474.

FOODY, G.M., CUTLER, M.E., McMORROW, J., PELZ, D., TANGKI, H., BOYD, D.S. and DOUGLAS, I., 2001, Mapping the biomass of Bornean tropical rain forest from remotely sensed data. *Global Ecology and Biogeography*, **10**, pp. 379–387.

GEIST, H.J. and LAMBIN, E.F., 2002, Proximate causes and underlying driving forces of tropical deforestation. *BioScience*, **52**, pp. 143–150.

GIBBS, H.K., BROWN, S., NILES, J.O. and FOLEY, J.A., 2007, Monitoring and estimating tropical forest carbon stocks: making REDD a reality. *Environmental Research Letters*, **2**, 045023, doi:10.1088/1748-93.

GOFC-GOLD (Ed.), 2009, *Reducing Greenhouse Gas Emissions from Deforestation and Degradation in Developing Countries: A Sourcebook of Methods and Procedures for Monitoring, Measuring and Reporting* (Edmonton, AB: GOFC-GOLD Project Office, Natural Resources Canada).

HAGNER, O. and REESE, H., 2007, A method for calibrated maximum likelihood classification of forest types. *Remote Sensing of Environment*, **110**, pp. 438–444.

HALL, F.G., BOTKIN, D.B., STREBEL, D.E., WOODS, K.D. and GOETZ, S.J., 1991, Large-scale patterns of forest succession as determined by remote-sensing. *Ecology*, **72**, pp. 628–640.

HANSEN, M.C., STEHMAN, S.V., POTAPOV, P.V., LOVELAND, T.R., TOWNSHEND, J.R.G., DEFRIES, R.S., PITTMAN, K.W., ARUNARWATI, B., STOLLE, F., STEININGER, M.K., CARROLL, M. and DIMICELI, C., 2008, Humid tropical forest clearing from 2000 to 2005 quantified by using multitemporal and multiresolution remotely sensed data. *Proceedings of the National Academy of Sciences*, **105**, pp. 9439–9444.

HEISKANEN, J., 2006, Estimating aboveground tree biomass and leaf area index in a mountain birch forest using ASTER satellite data. *International Journal of Remote Sensing*, **27**, pp. 1135–1158.

HENSON, I.E. and CHANG, K.C., 2003, Oil palm plantations & forest loss-an objective appraisal. In *Proceedings of the PIPOC 2003, International Palm Oil Congress*, 24–28 August, Putrajaya, Malaysia (Kuala Lumpur: Malaysian Palm Oil Board), pp. 960–974.

HOUGHTON, R.A. and HACKLER, J.L., 1999, Emissions of carbon from forestry and land-use change in tropical Asia. *Global Change Biology*, **5**, pp. 481–492.

HUETE, A.R., 1986, Separation of soil-plant mixtures by factor analysis. *Remote Sensing of Environment*, **19**, pp. 237–251.

HUETE, A.R., 1988, A soil-adjusted vegetation index (SAVI). *Remote Sensing of Environment*, **25**, pp. 295–309.

HUETE, A.R., DIDAN, K., MIURA, T., RODRIGUEZ, E.P., GAO, X. and FERREIRA, L.G., 2002, Overview of the radiometric and biophysical performance of the MODIS vegetation indices. *Remote Sensing of Environment*, **83**, pp. 195–213.

HUETE, A.R., LIU, H.Q., BATCHILY, K. and VAN LEEUWEN, W., 1997, A comparison of vegetation indices over a global set of TM images for EOS-MODIS. *Remote Sensing of Environment*, **59**, pp. 440–451.

ICRAF, 2008, Prosea agroforestry tree database: wood density database. World Agroforestry Centre. Available online at: http://www.worldagroforestry.org/sea/Products/AFDbases/WD/index.htm (accessed March 2009).

JACKSON, R.D. and HUETE, A.R., 1991, Interpreting vegetation indices. *Preventive Veterinary Medicine*, **11**, pp. 185–200.

JARVIS, A., REUTER, H.I., NELSON, A. and GUEVARA, E., 2006, *Hole-filled Seamless SRTM Data V3*. Available online at: http://srtm.csi.cgiar.org

JUSOFF, K. and PATHAN, M., 2009, Mapping of individual oil palm trees using airborne hyperspectral sensing: an overview. *Applied Physics Research*, **1**, pp. 15–30.

KARNIELI, A., KAUFMAN, Y.J., REMER, L. and WALD, A., 2001, AFRI- aerosol free vegetation index. *Remote Sensing of Environment*, **77**, pp. 10–21.

LEE, J.-S., 1980, Digital image-enhancement and noise filtering by use of local statistics. *IEEE Transactions on Pattern Analysis and Machine Intelligence*, **2**, pp. 165–168.

LU, D., 2005, Aboveground biomass estimation using Landsat TM data in the Brazilian Amazon. *International Journal of Remote Sensing*, **26**, pp. 2509–2525.

LU, D., BATISTELLA, M., MORAN, E. and MAUSEL, P., 2004a, Application of spectral mixture analysis to Amazonian land-use and land-cover classification. *International Journal of Remote Sensing*, **25**, pp. 5345–5358.

LU, D., MAUSEL, P., BRONDIZIO, E. and MORAN, E., 2004b, Relationships between forest stand parameters and Landsat TM spectral responses in the Brazilian Amazon Basin. *Forest Ecology and Management*, **198**, pp. 149–167.

Lu, D.S., 2006, The potential and challenge of remote sensing-based biomass estimation. *International Journal of Remote Sensing*, **27**, pp. 1297–1328.

Lu, D.S., Batistella, M. and Moran, E., 2005, Satellite estimation of aboveground biomass and impacts of forest stand structure. *Photogrammetric Engineering and Remote Sensing*, **71**, pp. 967–974.

Marsh, C.W. and Greer, A.G., 1992, Forest land-use in Sabah, Malaysia: an introduction to Danum Valley. *Philosophical Transactions – Royal Society of London, B*, **335**, pp. 331–339.

McDonald, A.J., Gemmell, F.M. and Lewis, P.E., 1998, Investigation of the utility of spectral vegetation indices for determining information on coniferous forests. *Remote Sensing of Environment*, **66**, pp. 250–272.

McMorrow, J., 2001, Linear regression modelling for the estimation of oil palm age from Landsat TM. *International Journal of Remote Sensing*, **22**, pp. 2243–2264.

McMorrow, J. and Talip, M.A., 2001, Decline of forest area in Sabah, Malaysia: relationship to state policies, land code and land capability. *Global Environmental Change-Human and Policy Dimensions*, **11**, pp. 217–230.

McMorrow, J.M., Lawes, H.M. and Mustapa, T., 1996, Monitoring tropical rain forest conversion to estate agriculture in Sabah Malaysia using Landsat images and GIS. In *Multiple Resource Inventory and Monitoring of Tropical Forests*, H.A. Hassan, Y.M. Chin and N. Rahman (Eds.) (Kuala Lumpur: ASEAN Institute of Forest Management).

Morel, A.C., Saatchi, S.S., Malhi, Y., Berry, N.J., Banin, L., Burslem, D., Nilus, R. and Ong, R.C., 2011, Estimating aboveground biomass in forest and oil palm plantation in Sabah, Malaysian Borneo using ALOS PALSAR data. *Forest Ecology and Management*, **262**, pp. 1786–1798.

Malaysian Palm Oil Board (MPOB), 2008, *Malaysian Oil Palm Statistics 2007*. Available online at: http://econ.mpob.gov.my/economy/annual/stat2007/EID_statistics07.htm (accessed 28 April 2008).

Murdiyarso, D., Noordwijk, M.V., Wasrin, U.R., Tomich, T.P. and Gillison, A.N., 2002, Environmental benefits and sustainable land-use options in the Jambi Transect, Sumatra. *Journal of Vegetation Science*, **13**, pp. 429–438.

Muukkonen, P. and Heiskanen, J., 2005, Estimating biomass for boreal forests using ASTER satellite data combined with standwise forest inventory data. *Remote Sensing of Environment*, **99**, pp. 434–447.

Myers, N., Mittermeier, R.A., Mittermeier, C.G., Da Fonseca, G.A.B. and Kent, J., 2000, Biodiversity hotspots for conservation priorities. *Nature*, **403**, pp. 853–858.

Nemani, R., Pierce, L., Running, S.W. and Band, L., 1993, Forest ecosystem processes at the watershed scale: sensitivity to remotely-sensed leaf area index estimates. *International Journal of Remote Sensing*, **14**, pp. 2519–2534.

Olander, L.P., Gibbs, H.K., Steininger, M., Swenson, J.J. and Murray, B.C., 2008, Reference scenarios for deforestation and forest degradation in support of REDD: a review of data and methods. *Environmental Research Letters*, **3**, 025011, doi:10.1088/1748-9326/3/2/025011.

Paoli, G.D., Curran, L.M. and Slik, J.W.F., 2008, Soil nutrients affect spatial patterns of aboveground biomass and emergent tree density in southwestern Borneo. *Oecologia*, **155**, pp. 287–299.

Patenaude, G., Milne, R. and Dawson, T.P., 2005, Synthesis of remote sensing approaches for forest carbon estimation: reporting to the Kyoto Protocol. *Environmental Science and Policy*, **8**, pp. 161–178.

Phua, M.-H. and Saito, H., 2003, Estimation of biomass of a mountainous tropical forest using Landsat TM data. *Canadian Journal of Remote Sensing*, **29**, pp. 429–440.

Richardson, A.J. and Everitt, J.H., 1992, Using spectral vegetation indices to estimate rangeland productivity. *Geocarto International*, **7**, pp. 63–69.

ROBERTS, D.A., SMITH, M.O. and ADAMS, J.B., 1993, Green vegetation, non-photosynthetic vegetation and soils in AVIRIS data. *Remote Sensing of Environment*, **44**, pp. 255–269.

ROUSE, J.W., HAAS, R.H., SCHELL, J.A. and DEERING, D.W., 1973, Monitoring vegetation systems in the Great Plains with ERTS. In *Proceedings of Third ERTS Symposium*, NASA, Washington, DC.

SADER, S.A., WAIDE, R.B., LAWRENCE, W.T. and JOYCE, A.T., 1989, Tropical forest biomass and successional age class relationships to a vegetation index derived from Landsat TM data. *Remote Sensing of Environment*, **28**, pp. 143–186.

SILLEOS, N.G., ALEXANDRIDIS, T.K., GITAS, I.Z. and PERAKIS, K. 2006. Vegetation indices: advances made in biomass estimation and vegetation monitoring in the last 30 years. *Geocarto International*, **21**, pp. 21–28.

SLIK, J.W.F., AIBA, S.-I., BREARLY, F.Q., CANNON, C.H., FORSHED, O., KITAYAMA, K., NAGAMASU, H., NILUS, R., PAYNE, J., PAOLI, G., POULSEN, A.D., RAES, N., SHEIL, D., SIDIYASA, K., SUZUKI, E. and VALKENBURG, J.L.C.H.V., 2010, Environmental correlates of tree biomass, basal area, wood specific gravity and stem density gradients in Borneo's tropical forests. *Global Ecology and Biogeography*, **19**, pp. 50–60.

SOUZA JR., C.M., ROBERTS, D.A. and COCHRANE, M.A., 2005, Combining spectral and spatial information to map canopy damage from selective logging and forest fires. *Remote Sensing of Environment*, **98**, pp. 329–343.

THENKABAIL, P.S., STUCKY, N., GRISCOM, B.W., ASHTON, M.S., DIELS, J., VAN DER MEER, B. and ENCLONA, E., 2004, Biomass estimations and carbon stock calculations in the oil palm plantations of African derived savannas using IKONOS data. *International Journal of Remote Sensing*, **25**, pp. 5447–5472.

TOU, J.T. and GONZALEZ, R.C., 1974, *Pattern Recognition Principles* (Reading, MA: Addison-Wesley Publishing Company).

TRIGG, S.N., CURRAN, L.M. and MCDONALD, A.K., 2006, Utility of Landsat 7 satellite data for continued monitoring of forest cover change in protected areas in Southeast Asia. *Singapore Journal of Tropical Geography*, **27**, pp. 49–66.

ÜNSALAN, C. and BOYER, K.L., 2004, Linearized vegetation indices based on a formal statistical framework. *IEEE Transactions on Geoscience and Remote Sensing*, **42**, pp. 1575–1585.

USGS, 2003, Landsat International Cooperators. United States Geological Survey. Available online at: http://international.usgs.gov/projects/prjlandsat.htm

USGS, 2006, *Shuttle Radar Topography Mission, 3 Arc Second: WRS-2 Scene SRTM_u50n_p116-117_r056-057, Unfilled Unfinished 2.0* (College Park, MD: Global Land Cover Facility, University of Maryland). Available online at: http://glcf.umiacs.umd.edu/data/srtm/index.shtml

VENNING, P., 2010, 'REDD' at the convergence of the environmental and development debates – international incentives for national action on avoided deforestation. *Law Environment and Development Journal*, **6**, p. 24.

VERMOTE, E.F., TANRE, D., DEUZE, J.L., HERMAN, M. and MORCRETTE, J.J., 1997, Second simulation of the satellite signal in the solar spectrum, 6S: an overview. *IEEE Transactions on Geoscience and Remote Sensing*, **35**, pp. 675–686.

WHITMORE, T., 1984, *Tropical Forests of the Far East*, 2nd ed. (Oxford: Oxford University Press).

WULDER, M.A., ORTLEPP, S.M., WHITE, J.C. and MAXWELL, S., 2008, Evaluation of Landsat-7 SLC-off image products for forest change detection. *Canadian Journal of Remote Sensing*, **34**, pp. 93–99.

YAMAKURA, T., HAGIHARA, A., SUKARDJO, S. and OGAWA, H., 1986, Aboveground biomass of tropical rain forest stands in Indonesian Borneo. *Vegetatio*, **68**, pp. 71–82.

ZELAZOWSKI, P., SAYER, A.M., THOMAS, G.E. and GRAINGER, R.G., 2011, Reconciling satellite-derived atmospheric properties with fine-resolution land imagery: insights for atmospheric correction. *Journal of Geophysical Research*, **116**, D18308, doi:10.1029/2010JD015488.

ZHANG, C., LI, W. and TRAVIS, D., 2007, Gaps-fill of SLC-off Landsat ETM plus satellite image using a geostatistical approach. *International Journal of Remote Sensing*, **28**, pp. 5103–5122.

ZHENG, D., HEATH, L.S. and DUCEY, M.J., 2008, Identifying grain-size dependent errors on global forest area estimates and carbon studies. *Geophysical Research Letters*, **35**, p. 5.

ZHENG, D.L., RADEMACHER, J., CHEN, J.Q., CROW, T., BRESEE, M., LE MOINE, J. and RYU, S.R., 2004, Estimating aboveground biomass using Landsat 7 ETM+ data across a managed landscape in northern Wisconsin, USA. *Remote Sensing of Environment*, **93**, pp. 402–411.

ZHENG, G., CHEN, J.M., TIAN, Q.J., JU, W.M. and XIA, X.Q., 2007, Combining remote sensing imagery and forest age inventory for biomass mapping. *Journal of Environmental Management*, **85**, pp. 616–623.